Interface porosity in multilayered all-conducting polymer electrodes

Nuria Borras,[1,*] Francesc Estrany,[1,2,*] and Carlos Alemán[1,2,*]

[1] *Departament d'Enginyeria Química, EEBE, Universitat Politècnica de Catalunya, C/ Eduard Maristany 10-14, Ed. I2, 08019, Barcelona, Spain.*

[2] Barcelona *Research Center in Multiscale Science and Engineering, Universitat Politècnica de Catalunya, C/ Eduard Maristany, 10-14, 08019, Barcelona, Spain*

[*] *nuria.borras@upc.edu*, *francesc.estrany@upc.edu* and *carlos.aleman@upc.edu*

ABSTRACT

Multilayered films made with at least two different electroactive polymers, in which the least conducting one acts as a dielectric and separates the layers made with the other, behave as efficient electrodes for electrochemical supercapacitors. In this work, we present a simple strategy to develop improved multilayered electrodes with structured interfaces by enhancing the porosity of the dielectric. This has been achieved by growing sodium chloride crystals onto a conducting polymer layer and, after generation of all required layers using the layer-by-layer electrodeposition technique, salt crystals have been eliminated by water-etching. Results from morphological and topographical studies on single-layered poly(3,4-ethylenedioxythiophene) (PEDOT), poly(N-methylpyrrole) (PNMPy) and poly(3,4-ethylenedioxythiophene-*co*-N-methylpyrrole) (COP), as well as electrochemical investigations on bi-layered films with enhanced porosity at the interface between the two layers, have been used to design new 4-layered electrodes. These consist in two layers of PEDOT separated by two-layers of nanosegregated COP with a porous interface in the middle. Although the properties of the new 4-layered electrodes improve due to the porous interface, the highest specific capacitance corresponds to the 2-layered electrode in which two PEDOT layers are separated by an ultra-porous interface.

INTRODUCTION

Supercapacitors have attracted a great interest over the past decade because of their high power capacity, fast energy uptake and delivery, long cycle life, simple principles, and low sensitivity to temperature and maintenance cost.[1] Charge storage in a supercapacitor device can be achieved through a double-layer electrostatic mechanism (*i.e.* adsorption and desorption of charged ions from an electrolyte onto highly porous electrodes) and/or a faradic redox process (*i.e.* pseudocapacitance that is based on fast and reversible surface redox reactions). Pseudocapacitors made of nanostructured conducting polymers (CPs), which store charge via rapid reduction and oxidation reactions, are particularly interesting since these materials combine the properties associated to conventional properties and the unique electronic characteristics of metals and semiconductors.[2-8]

In the last decade we used the layer-by-layer (LbL) electrodeposition technique to prepare nanostructured conducting systems based on three alternated layers of poly(3,4-ethylenedioxythiophene) (PEDOT) and poly(N-methylpyrrole) (PNMPy),[9-15] hereafter abbreviated 3l-PEDOT/PNMPy (*i.e.* PEDOT/PNMPy/PEDOT). These multilayered materials showed better electrochemical properties and a higher ability to store charge than each of the two individual CPs and the corresponding copolymer, poly(3,4-ethylenedioxythiophene-*co*-N-methylpyrrole), hereafter named COP.[16] Such improvement was attributed not only to the dielectric breakage effect promoted by the PNMPy intermediate sheet (*i.e.* the electrical conductivity is ~10^5 S/cm higher for PEDOT than for PNMPy) but also to the synergistic effects produced by the favorable interaction between the PEDOT and PNMPy layers at the interfaces. This synergy was proved considering 3-layered systems with different physical characteristics, composition and/or polymerization conditions. These included systems that differ in the

thickness of the layers (*i.e.* micro-[9-12] and nanometric[12-15] layers), systems prepared using dynamical conditions rather than conventional quiescent solutions,[10] and systems modified with clays at the dielectric layer[11] or with an octanethiol self-assembled monolayer at the first PEDOT layer.[15]

On the other hand, 3-layered electrodes has been also prepared replacing the PNMPy dielectrics by COP,[12] poly(indole-5-carboxylic acid),[17] poly[5,5'-bis(2,3-dihydrothieno[3,4-b][1,4]dioxin-5-yl)-2,2'-bithiophene].[18] Results obtained for PEDOT/COP/PEDOT 3-layered systems, hereafter after denoted 3l-PEDOT/COP were particularly noticeable since the copolymer organized forming nanophase segregated structures.[12] Accordingly, the intermediate layer of 3l-PEDOT/COP was described as a random disposition of ultrathin dielectrics having nanometric length and width. In terms of charge storage, the intermediate layer of 3l-PEDOT/COP was viewed as a thin reservoir filled of heterogeneously distributed nanometric supercapacitors that are connected in series among them and in parallel to the PEDOT layers.[12]

In this work we propose a capacitive 4-layered system as an improvement of the recently reported 3l-PEDOT/COP films.[12] The advantage of such new system, in which the LbL technique is used to electrodeposit two consecutive of COP layers (*i.e.* a double-dielectric sheet) between and two electroactive PEDOT layers (*i.e.* PEDOT/COP/COP/PEDOT), is the creation of a nanostructured interface in the middle of the dielectric. More specifically, the intermediate COP layer of 3l-PEDOT/COP is replaced by COP/p/COP, where p refers the ultra-porous interface separating the two consecutively deposited COP layers. Such substitution, which enhances the dielectric breakage between the external and the internal PEDOT layers, is achieved by growing sodium chloride (NaCl) crystals in the middle of the two COP layers, COP/NaCl/COP. Once the system with four CP layers is completed (PEDOT/COP/NaCl/COP/PEDOT),

salt crystals are eliminated by water-etching. It is worth noting that, although NaCl was exploited as dopant agent,[19-23] it has been never used as template to modify the properties and the structure of the dielectric separating two electroactive layers. In order to provide a rational understanding of the experimental observations, results have been organized in three blocks according to the increasing number of layers in the films: *i)* morphological and topographical properties of single-layered films; *ii)* electrochemical and capacitive properties of 2-layered films; and *iii)* electrochemical and capacitive properties of 4-layered systems.

METHODS

Materials. 3,4-ethylenedioxythiophene (EDOT), N-methylpyrrole (NMPy) and acetonitrile were purchased from Sigma-Aldrich (Spain) and used as received, whereas NaCl (reagent grade) was purchased from Scharlau. Anhydrous lithium perchlorate ($LiClO_4$) was purchased from Sigma-Aldrich (Spain) and was stored in an oven at 80 ºC before use in the electrochemical trials. All chemicals were analytical reagent grade.

Synthesis of PEDOT, PNMPy and COP single-layered films. Films were prepared by chronoamperometry (CA) under a constant potential of 1.40 V and adjusting the polymerization charge to 0.55 C. All polymerizations were conducted in a three-electrode one-compartment cell under nitrogen atmosphere (99.995% in purity) at 25 ºC. Steel AISI 316 sheets of 1×1.5 cm^2 area were employed as working and counter electrodes. To avoid interferences during the electrochemical analyses, before each trial the working and counter electrodes were cleaned with ethanol, after that with acetone, and dried in an air-flow. The reference electrode was an Ag|AgCl electrode containing a

KBr saturated aqueous solution (E^o = 0.222 V vs. standard hydrogen electrode at 25 ºC). All the potentials reported in this work are referred to the Ag|AgCl electrode.

PEDOT and PNMPy films were prepared filling the cell with 40 mL of a 10 mM acetonitrile solution of the corresponding monomer with 0.1 M $LiClO_4$ as doping electrolyte. In the case of COP, the concentration of EDOT and NMPy in reaction medium was 5 mM each. NaCl crystals were grown by immersing the prepared films in a 20% w/v salt aqueous solution for 5 s and, subsequently, leaving them in a desiccator overnight for drying. Hereafter, the resulting single-layered films are denoted: CP/NaCl, where CP= PEDOT, PNMPy or COP. Finally, films with a porous surface were obtained by removing the grown salt crystals from CP/NaCl by simple water-etching. For this purpose, CP/NaCl films were immersed in water overnight and, subsequently, maintained in a desiccator 24 h for drying, the resulting films being denoted CP/p, where p refers to porous. Figure 1a schematizes the process used to prepare pristine PEDOT, PEDOT/NaCl and PEDOT/p films. All electrochemical experiments were conducted on a PGSTAT302N AUTOLAB potentiostat-galvanostat connected to a PC computer and controlled through the NOVA 1.6 software.

Synthesis of PEDOT or PNMPy 2-layered films. Films containing two layers of the same homopolymer (*i.e.* PEDOT or PNMPy) were prepared by immersing the steel AISI 316 electrode coated with a single-layered CP or CP/NaCl film, obtained as described above, in a cell filled with 10 mM acetonitrile solution of the corresponding monomer (*i.e.* EDOT or NMPy) with 0.1 M $LiClO_4$. Then, an electropolymerization was conducted under a constant potential of 1.40 V and adjusting the polymerization charge to 0.55 C. The resulting 2-layered films were denoted CP/CP (blank) or CP/NaCl/CP with CP= PEDOT or PNMPy. In order to eliminate the NaCl crystals,

CP/NaCl/CP films were immersed in water overnight and, subsequently, maintained in a desiccator 24 h for drying. The resulting 2-layered films, named CP/p/CP (where p refers to the artificially created porous interface), were symmetric from a chemical point of view since they contained two layers made with the same CP, even though they were separated by porous and heterogeneous interface. Figure 1b shows the process used to prepare PEDO/NaCl/PEDOT and PEDOT/p/PEDOT films.

Synthesis of PEDOT and COP 4-layered films. Films containing two PEDOT layers separated by COP/COP, COP/NaCl/COP or COP/p/COP were prepared by immersing the steel AISI 316 electrode coated with the corresponding single-layered PEDOT film in a cell filled with a 5 mM NMPy-, 5 mM EDOT- and 0.1 M $LiClO_4$-containing acetonitrile solution. A COP layer was electrogenerated onto the PEDOT film by CA under a constant potential of 1.40 V and adjusting the polymerization charge to 0.55 C. The same process was used to coat the resulting 2-layered film, PEDOT/COP, with another COP layer directly or after growing NaCl crystals, as described previously. Finally, another PEDOT layer was added applying the same procedure. The resulting multilayered films were named PEDOT/COP/COP/PEDOT and PEDOT/COP/NaCl/COP/PEDOT, respectively, the latter transforming into PEDOT/COP/p/COP/PEDOT after remove the inorganic crystals with water. The procedure used to prepare PEDOT/COP/NaCl/COP/PEDOT and PEDOT/COP/p/COP/PEDOT is schematized in Figure 1c.

Surface characterization. Scanning electron microscopy (SEM) studies were performed to examine the surface morphology of the prepared single-layered films.

Dried samples were placed in a Focussed Ion Beam Zeiss Neon 40 scanning electron microscope operating at 3 kV, equipped with an EDX spectroscopy system.

Atomic force microscopy (AFM) images were obtained with a Molecular Imaging PicoSPM using a NanoScope IV controller under ambient conditions. The tapping mode AFM was operated at constant deflection. AFM was operated in ambient conditions at a scan speed of 1 Hz in all cases. Measurements were performed on various parts of the films, which provided reproducible images similar to those displayed in this work. The statistical application of the NanoScope Analysis software was used to determine the root mean square roughness (Rq), which is the average height deviation taken from the mean data plane. The scan window sizes were 10×10 μm^2 in all cases.

FTIR and UV-vis spectroscopies. FTIR spectra were recorded on a Bruker Vertex 70 FTIR spectrometer, equipped with a diamond ATR device (Golden Gate, Bruker) in transmission mode, by using KBr pellets.

UV-vis absorption spectra were obtained using a UV-vis-NIR Shimadzu 3600 spectrophotometer equipped with a tungsten halogen visible source, a deuterium arc UV source, a photomultiplier tube UV-vis detector, and a InGaAs photodiode and cooled PbS photocell NIR detectors. Spectra were recorded in the absorbance mode using the integrating sphere accessory (model ISR-3100), the range wavelength being 200–900 nm. The interior of the integrating sphere was coated with highly diffuse $BaSO_4$ reflectance standard. Single-scan spectra were recorded at a scan speed of 60 nm/min. Measurements, data collection and data evaluation were controlled by the computer software UVProbe version 2.31.

Electrochemical characterization. All electrochemical experiments were run in triplicate using an acetonitrile solution with 0.1 M $LiClO_4$ as supporting electrolyte. Cyclic voltammetry (CV) was carried out to evaluate the electroactivity, specific capacitance (*SC*) and the electrochemical stability of the prepared electrodes. The initial and final potentials were –0.50 V, and the reversal potential was 1.60 V. The number of oxidation-reduction cycles applied was 50. A scan rate of 50 mV/s was used in all cases.

The electrochemical activity was evaluated through the voltammetric charge corresponding to the 2nd oxidation-reduction cycle (Q_{2nd}; in C). The *SC* (in F/g) was determined from the registered voltammograms using the following Eq:

$$SC = \frac{Q}{\Delta V \cdot m} \quad (1)$$

where Q is the voltammetric charge, ΔV is the potential window (in V), and m is the mass of CP on the surface of the working electrode (in g). Finally, the electrochemical stability was estimated as the reduction of the *SC* after 50 consecutive oxidation-reduction cycles (ΔSC; in %).

RESULTS AND DISCUSSION

Morphological studies on single-layered films

Figure 2 displays SEM micrographs of PEDOT, PEDOT/NaCl and PEDOT/p. Pristine PEDOT films present the typical clustered morphology with small aggregates connected by dense networks of thin fiber-like structures (Figure 2a). This porous morphology is expected to facilitate the access and escape of dopant ions during oxidation and reduction processes, respectively. 3D topographic and 2D height AFM images (Figure 3a), which show aggregation of small clusters over the polymer surface, corroborate SEM observations. The root mean square roughness (Rq) determined for

this system is Rq= 674 nm while the size of the aggregates is ~2 μm, as is shown by the cross-sectional profile of the surface topography included in Figure 3a.

Immersion of pristine PEDOT in NaCl solution resulted in the formation of micrometric inorganic crystals at the surface that grew among already formed CP clusters, as shown in Figure 1a. Moreover, SEM micrographs recorded for PEDOT/NaCl (Figure 2b) suggest that NaCl crystals are abundant. Representative AFM images displayed in Figure 3b indicate that in many cases crystals are partially embedded in the CP matrix, evidencing the integration of the two materials. This feature is confirmed by the corresponding cross-sectional profile (Figure 3b), which flows without discontinuities at the crystal-PEDOT interface.

Elimination of NaCl through solvent etching to produce PEDOT/p induced an increment in the surface porosity with respect to pristine PEDOT. Thus, the stress exerted on the CP by the growing inorganic crystals caused some distortions in the polymer network. Throughout this process, the surface of the CP, which behaved as a mold, changed and pores were opened. The structural distortions induced by this mold effect transformed into pores once the NaCl crystals were dissolved by water, as shown clearly in the SEM micrographs of Figure 2c. The enhancement of the surface porosity motived a drastic increment in the surface roughness that, unfortunately, precluded the proper acquisition of satisfactory AFM images for PEDOT/p films.

Representative SEM micrographs of PNMPy, PNMPy/NaCl and PNMPy/p single-layered films are displayed in Figure 4. Pristine PNMPy films (Figure 4a) present a very compact globular morphology formed by a homogeneous distribution of pseudo-spherical particles of different sizes (*i.e.* from ~100 to ~400 nm). Many of such globular particles are fused forming dense aggregates, which in turn pack very compactly forming an impenetrable surface without pores. On the other hand, NaCl crystals are

clearly detected in the surface of PNMPy/NaCl films (Figure 4b), even though the growth of such crystals is clearly different to that observed in PEDOT/NaCl (Figure 2b). More specifically, NaCl crystals grew onto the surface of the PNMPy film without penetrate into the polymer matrix due to the lack of pores. Consequently, the surface morphology of the PNMPy/p film, once the crystals are removed with water, is similar to that of the pristine CP, as is clearly observed in Figure 4c.

Topographic and phase AFM images of PNMPy, PNMPy/NaCl and PNMPy/p (Figure 5), which exhibit Rq values of 240, 580 and 310 nm, respectively, are fully consistent with SEM observations. As it can be seen, PNMPy/p retains the globular topography of pristine PNMPy, even though the roughness of the latter is slightly higher. Besides, the different viscoelastic response of the PNMPy matrix and the NaCl crystals is clearly identified in the phase image of PNMPy/NaCl (Figure 5b).

SEM micrographs and AFM images of COP-based single-layered films are displayed in Figures 6 and 7, respectively. Pristine COP films show a surface morphology that is intermediate between those described for the two homopolymers. More specifically, the morphology of COP can be described as the superposition of the homogeneous globular and compact structure identified for PNMPy and the clustered heterogeneous distribution found for PEDOT (Figure 6a). This feature suggests that the EDOT- and NMPy-blocks in the copolymer distribute in separated phases, capturing the most characteristic structural trends of the two homopolymers. This assumption is supported by the contrast in the phase image included in Figure 7a, which differentiates the EDOT- and NMPy-rich phases in pristine COP films. Thus, the EDOT-rich phase should be visualized as PEDOT with some dissolved PNMPy while the NMPy-rich phase should be represented as PNMPy with some dissolved PEDOT. Moreover, these leveled organization resulted in a Rq value of 316 nm, which is intermediate between

those of heterogeneous PEDOT (Rq= 674 nm) and globular PNMPy films (Rq= 240 nm).

Immersion in NaCl aqueous solution results in the formation of a multitude of submicron crystals (Figure 6b). Thus, the coexistence of two phases in the COP film determined the nucleation and growth of the NaCl crystals. More specifically, crystals nucleated at the EDOT-rich phase grew embedded into the more porous polymeric matrix while those located at the NMPy-rich phase were simply deposited onto the polymeric surface, as occurred in the corresponding homopolymer films. However, the growth of the crystals was restricted by the distribution of the two phases and, therefore, crystals were much smaller in COP/NaCl than in PEDOT/NaCl and PNMPy/NaCl. In addition, the small size of the formed inorganic crystals is clearly evidenced in the 3D topographic and 2D phase contrast AFM images of COP/NaCl (Figure 7b). This observation is supported by the surface roughness of COP/NaCl, Rq= 359 nm, which only increased 14% with respect to pristine COP.

Finally, inspection of SEM micrographs and AFM images of COP/p, which are shown in Figures 6c and 7c, respectively, suggests an increment of the surface porosity in the EDOT-rich phases while the NMPy-rich phases remain compact. Although crystals are much smaller in COP/p than in PEDOT/p, the increment in the surface porosity of the former should be attributed to the stress exerted by the growing of inorganic crystals nucleated on the EDOT-rich phases. This stress, which is caused by the partial embedment of the NaCl crystals in the EDOT-rich matrix, induces a remarkable opening of the superficial pores and, consequently, a notable increment of the surface roughness (Rq= 753 nm).

Spectroscopic studies on 2-layered films

The FTIR spectra of PEDOT/PEDOT, PEDOT/NaCl/PEDOT and PEDOT/p/PEDOT films are compared in Figure 8a. As it can be seen, the main bands in the spectra are very similar for the three 2-layered films, even though the resemblance is higher between PEDOT/PEDOT and PEDOT/p/PEDOT because of the noise introduced by NaCl crystals in PEDOT/NaCl/PEDOT. The most relevant bands correspond to the CH_2 stretching at 750 cm^{-1}, C–O–C vibrations at 1205 and 1078 cm^{-1}, the stretch of the C–S bond in the thiophene ring at 871 and 681 cm^{-1}. These results indicate that NaCl is not producing any chemical change in the structure of PEDOT but only physical changes at the structure of the interface between the two layers.

The UV-vis spectra displayed in Figure 8b exhibits a broad absorption tail between ~420 and ~800 nm for PEDOT/PEDOT, PEDOT/NaCl/PEDOT and PEDOT/p/PEDOT ascribed to the polaronic band of the conductive quinoid form. This optical transition of is very similar to that reported for single layered films PEDOT and several of its derivatives, as was previously discussed in detail.[31,32]

Voltammetric studies on 2-layered films

In order to ascertain if the PNMPy and COP dielectric layer of 3l-PEDOT/PNMPy and 3l-PEDOT/COP electrodes, respectively, can be completely replaced by an ultraporous interface between the two PEDOT layers, the main electrochemical properties of PEDOT/PEDOT, PEDOT/NaCl/PEDOT and PEDOT/p/PEDOT 2-layered films were examined. Table 1 lists the following electrochemical parameters: *i*) the voltammetric charge and the specific capacitance after two consecutive oxidation-reduction cycles (Q_{2nd} and SC_{2nd}, respectively); *ii*) the specific capacitance after fifty redox cycles (SC_{50th}); and *iii*) the reduction of the specific capacitance after fifty redox cycles with respect to SC_{2nd} (ΔSC), as a measure of the electrochemical stability.

Both Q_{2nd} and SC_{2nd} are ~5% higher for PEDOT/NaCl/PEDOT than for PEDOT/PEDOT, which have been attributed to the participation of Cl^- anions coming from NaCl crystals in the oxidation and reduction processes. Elimination of the inorganic crystals with water results in a very porous interface (Figure 2c) that facilitates the exchange of ions with the medium. Consequently, the interface that separates the two CP layers in PEDOT/p/PEDOT causes an increment of ~19% in both Q_{2nd} and SC_{2nd} with respect to PEDOT/PEDOT. On the other hand, the SC_{2nd} determined for 3l-PEDOT/PNMPy[24] and 3l-PEDOT/COP[12] single electrodes was of 35 and 72 F/g, respectively. Accordingly, the replacement of the PNMPy or COP dielectric layer by a porous interface between the two PEDOT layers enhances the charge storage capacity by 151% and 22%, respectively. In spite of these increments, the performance of the PEDOT/p/PEDOT electrode is worse than that of electrodes obtained using nanocomposite made of PEDOT and inorganic materials (*e.g.* MnO_2, MoO_3, carbon nanotubes, V_2O_5 and $NiFe_2O_4$). Thus, the SC_{2nd} values for such nanocomposite electrodes typically range from 150 to 400 F/g,[25-30] evidencing the benefits associated to the incorporation of additional inorganic components. However, the improvement achieved in PEDOT/p/PEDOT is exclusively based on the increment of the specific surface area, which is precisely also a basic requirements for obtaining good capacitive properties. Within this context, it should be noted that the capacitance of porous electrodes developed in this work is comparable or even higher than that of carbon electrodes frequently used in commercial supercapacitors.

Figure 9a compares the control voltammograms recorded for the oxidation of PEDOT/PEDOT, PEDOT/NaCl/PEDOT and PEDOT/p/PEDOT films in acetonitrile 0.1 M $LiClO_4$ for the potential window comprised between –0.50 V (initial and final potential) and 1.60 V (reversal potential). PEDOT/PEDOT shows two consecutive

oxidation peaks, the first one with the potential peak at 0.6 V and the second one overlapping with the oxidation potential of the medium. In addition, two reduction peaks with potential peaks at 0.8 and 0.1 V are detected in the cathodic scanning, indicating the presence of redox pairs in the recorded potential range. The total reduction charge is ~83% of the total oxidation charge, as determined from the oxidation of the cathodic and anodic areas, reflecting a quasi-reversible reduction pair. Oxidation and reduction peaks are much less defined in the control voltammogram of PEDOT/NaCl/PEDOT. This has been attributed to the delocalization of the corresponding oxidation and reduction potentials, which is induced by the NaCl crystals. Similarly, the voltammogram recorded for PEDOT/p/PEDOT is less defined and shows higher cathodic and anodic areas than that obtained for PEDOT/PEDOT, which suggest the existence of a remnant effect after dissolution of the NaCl crystals. Although they are less pronounced, the changes observed in PEDOT/p/PEDOT with respect PEDOT/PEDOT remind to those previously observed for multilayered films of PEDOT and PNMPy when the number of layers gradually increased from 3 to 7.[33] Accordingly, cyclic voltammograms displayed in Figure 9a suggest that the porous interface between the two PEDOT layers tends to behave as an intermediate dielectric layer.

The electrochemical stability was evaluated by submitting the prepared bi-layered films to 50 consecutive oxidation-reduction cycles in the potential interval comprised between –0.50 V and 1.60 V. It is worth noting that this is a very aggressive assay since the potential window is very large and, therefore, a drastic structural degradation of the CP is expected. Figure 9a includes the 50^{th} cycle recorded for PEDOT/PEDOT, PEDOT/NaCl/PEDOT and PEDOT/p/PEDOT, evidencing that both the cathodic and anodic areas experience a reduction in comparison to the corresponding first control

voltammograms. However, this effect is more pronounced for PEDOT/PEDOT and PEDOT/NaCl/PEDOT than for PEDOT/p/PEDOT. Furthermore, the Δ*SC* determined for PEDOT/PEDOT, PEDOT/NaCl/PEDOT and PEDOT/p/PEDOT is 57%, 33% and 27%, respectively (Table 1), indicating that the electrochemical stability is more than twice for the latter than for the former. Consistently, the SC_{50th} of PEDOT/p/PEDOT is more than twice that of PEDOT/PEDOT and only 14% lower than the SC_{2nd} measured for PEDOT/PEDOT. Overall, these results clearly reflect that the electrochemical performance of PEDOT/p/PEDOT is higher than that of the pristine 2-layered CP film not only in terms of *SC* but also in terms of electrochemical stability. This has been attributed to very porous interface separating the two PEDOT layers that actually behaves as a small dielectric layer.

In order to confirm that the exceptional behavior of PEDOT/p/PEDOT is due to the unique structure of the interface separating the two layers, PNMPy/PNMPy, PNMPy/NaCl/PNMPy and PNMPy/p/PNMPy were also studied. Figure 9b and Table 1 shows the control voltammograms and electrochemical parameters, respectively, for such 2-layered films. PNMPy/PNMPy shows two consecutive oxidation peaks. The first appears at 0.6 V while the second overlaps with the oxidation potential of the medium. The cathodic scan shows a reduction peak at 0.5 V, indicating the formation of electroactive polarons in the range of potentials investigated. Although the Q_{2nd} is 19% lower for PNMPy/PNMPy than for PEDOT/PEDOT, the SC_{2nd} of the former is 15% higher than that of the latter. This should be attributed to the fact that the current productivity (*i.e.* electrical charge consumed to produce a unit of polymer mass) is lower for PNMPy than for PEDOT (*i.e.* 0.619 and 0.875 mg/C, respectively).

Incorporation of NaCl at the interface between the two PNMPy layers results in a drastic increment of the SC_{2nd}, which is ~52% higher than for PNMPy/PNMPy. This has

been attributed to the coexistence of two factors: 1) PNMPy presents a very compact morphology, which makes difficult the exchange of ClO_4^- dopant ions with the medium during redox processes; and 2) the effective diameter of the Cl^- ions supplied by NaCl crystals is smaller than that of ClO_4^- dopant ions used in the synthesis of PNMPy films. Accordingly, the substitution of ClO_4^- by Cl^- as dopant ion in PNMPy/NaCl/PNMPy could explain the remarkable increment of both Q_{2nd} and SC_{2nd} with respect to PNMPy/PNMPy. This behavior is completely different from that observed for PEDOT/NaCl/PEDOT and PEDOT/PEDOT, which presented an intrinsic large porosity and, consequently, a great facility to exchange medium size ions. Besides, the control voltammogram of PNMPy/NaCl/PNMPy also shows the oxidation and reduction peaks identified for PNMPy/PNMPy, even though they shifted to 1.3 and –0.3 V because of the exchange of dopant ions.

Oxidation and reduction peaks are significantly more pronounced in the control voltammogram of PNMPy/p/PNMPy. This has been attributed to the complete substitution of ClO_4^- by Cl^-, the mobility being significantly greater for the latter than for the former. Thus, in this case the role played by the porosity originated at the interface between the two PNMPy layers is negligible because of the very compact morphology of this CP (Figures 4 and 5). Indeed, the Q_{2nd} and SC_{2nd} are lower for PNMPy/p/PNMPy (Table 1) than for PNMPy/PNMPy by 69% and 49%, respectively.

Finally, inspection to the SC_{50th} (Table 1) indicates a reduction of 68%, 24% and 49%, respectively, with respect to the corresponding SC_{2nd} values, Thus, the electrochemical stability of PNMPy/PNMPy and PNMPy/p/PNMPy is lower than that of the PEDOT-containing analogues because of both the compact structure of PNMPy and its tendency to form cross-links when a potential scan is applied.[34] Obviously, this degradative effect is not possible for PEDOT/PEDOT and PEDOT/p/PEDOT. An

exception to this behavior is detected for PNMPy/NaCl/PNMPy since in this case ΔSC is of only 23%. This has been attributed to the overoxidation induced by the continuous supply of dopant ions from the NaCl crystals to the CP.

Voltammetric studies on 4-layered CP films

Analysis of the results discussed in previous subsections suggests that the best location for the porous interface is the COP layer since it agglutinates the benefits of PEDOT and PNMPy. Accordingly, in this section we examine a 4-layered electrode that, indeed, is an extension of 3l-PEDOT/COP.[12] More specifically, the COP layer of 3l-PEDOT/COP has been replaced by COP/p/COP to introduce the porous interface just in the middle and, therefore, maximize the dielectric rupture. Accordingly, the four layers of the new designed electrode are distributed as follows two layers of PEDOT separated by two-layers of nanosegregated COP with a porous interface in the middle (*i.e.* PEDOT/COP/p/COP/PEDOT).

Figure 10 displays the cyclic voltammograms recorded for PEDOT/COP/COP/PEDOT (blank), PEDOT/COP/NaCl/COP/PEDOT and PEDOT/COP/p/COP/PEDOT. In general, they have characteristics that arise from the combination of those presented in Figure 9, which is fully consistent with the blocks segregated structure attributed to the copolymer. The PEDOT/COP/COP/PEDOT film shows an smooth oxidation peak at 0.9 V, which shifts to 0.5 V in the PEDOT/COP/NaCl/COP/PEDOT one. As is typically observed in multilayered systems, the peak is very weak for PEDOT/COP/COP/PEDOT and practically disappears for PEDOT/COP/p/COP/PEDOT. Moreover, none reduction peak is observed in 4-layered films. However, the most striking results obtained for the 4-layered systems are included in Table 1. Comparison of PEDOT/COP/COP/PEDOT with

PEDOT/COP/p/COP/PEDOT reveals that the creation of the porous interface in the middle of the dielectric increases the SC_{2nd} and SC_{50th} by 24% and 39%, respectively. Thus, the ΔSC decreases from –26% to –17%. According to these measures, the interface created in the dielectric layer improves not only the ability to store charge but also the electrochemical stability.

On the other hand, the SC_{2nd} of PEDOT/COP/p/COP/PEDOT is about half of that of PEDOT/p/PEDOT but ~10% higher than that of PNMPy/p/PNMPy. These observations have been attributed to the electrochemical activity of the three CPs which decreases as follows: PEDOT >> COP > PNMPy. In contrast, the ΔSC of PEDOT/p/PEDOT and PNMPy/p/PNMPy was –27% and –49%, respectively, while that of PEDOT/COP/p/COP/PEDOT decreased to –17% only. This feature indicates that the enhancement of the porosity in the middle of the nanosegregated dielectrics interface enhances considerably the electrochemical stability of the COP and, therefore, the utilization of COP/p/COP improves considerably the stability of PEDOT-based electrodes.

CONCLUSIONS

In this work we demonstrate the great potential of the interface porosity in the preparation of multilayered electrodes for supercapacitor applications. This porosity, which can be easily induced by growing NaCl crystals at the interface between two consecutive CP layers, causes structural distortions in the CP polymer network. The pores of the CP, which behaves as a deformable mold, are more opened once the NaCl is etched with water. Among, the different 2- and 4-layered systems studied in this work, two of them deserve special attention. The first one is the PEDOT/p/PEDOT, in which the intrinsically porous structure of PEDOT is enhanced by the NaCl crystals,

becoming ultra-porous. This causes an increase of 19% in the SC_{2nd} with respect to PEDOT/PEDOT. The second is the PEDOT/COP/p/COP/PEDOT, in which the phase-segregated structure of COP in PEDOT/COP/PEDOT is changed by COP/p/COP. This 4-layered system combines the benefits associated to the organization of COP in NMPy- and EDOT-rich domains and the formation of a porous interface in the middle of the dielectrics. The SC_{2nd} is 24% higher for PEDOT/COP/p/COP/PEDOT than for PEDOT/COP/COP/PEDOT due to the porosity enhancement. Overall, results indicate that the incorporation of porous interfaces by growing water soluble inorganic crystals is a promising general approach that can be used to improve the performance of CP-based supercapacitors.

ACKNOWLEDGEMENTS

Authors acknowledge MINECO/FEDER (MAT2015-69367-R) and the Agència de Gestió d'Ajuts Universitaris i de Recerca (2017SGR359). Support for the research of C.A. was received through the prize “ICREA Academia” for excellence in research funded by the Generalitat de Catalunya.

AUTHOR CONTRIBUTIONS

N. Borras, F. Estrany and C. Alemán participated in the conceptual design. N. Borras and F. Estrany performed experimental studies. C. Alemán drafted the paper. All the authors discussed and reviewed the final version.

REFERENCES

1. Yan, J., Wang, Q., Wei T. and Fan, Z. *Adv. Energy Mater*. **2014**, *4*, 1300816.

2. Shi, Y., Peng, L., Ding, Y., Zhao, Y. and G. Yu, *Chem. Soc. Rev.* **2015**, *44*, 6684–6696.
3. Bryan, A. M., Santino, L. M., Lu, Y., Acharva, S. and D'Arcy, J. M. *Chem. Mater.* **2016**, *28*, 5989–5998.
4. Yang, J., Liu, Y., Li, L., Zhang, C. and Liu, T. *Mater. Chem. Front.* **2017**, *1*, 251–268.
5. Yang, J., Liu, Y., Liu, S., Li, L., Zhang, C. and Liu, T. *Nanomaterials* **2015**, *5*, 906–936.
6. Ghosh, S., Maiyalagan, T., Basu, R. N. *Nanoscale* **2016**, *8*, 6921–6947.
7. Ambade, R. A., Ambade, S. B., Salunke, R. R., Malgras, V., Jin, S. H., Yamauchi, Y. and Lee, S.-H. *J. Mater. Chem. A* **2016**, *4*, 7406–7415.
8. Nguyen, D. N. and Yoon, H. *Polymers* **2016**, *8*, 118
9. Aradilla, D., Estrany, F., Casellas, F., Iribarren, J. I. and Alemán, C. *Org. Electron.* **2014**, *15*, 40–46.
10. Sánchez-Jiménez, M., Alemán, C. and Estrany, F. *Polym. Eng. Sci.* **2014**, ***54***, 2121–2131.
11. Amoura, D., Sánchez-Jiménez, M., Estrany, F., Makhloufi, L. and Alemán, C. *Eur. Polym. J.* **2015**, **69**, 296–307.
12. Borras, N., Estrany, F. and Alemán, C. *Org. Electron.* **2017**, *51*, 322–331.
13. F. Estrany, Aradilla, D., Oliver, R., Armelin, E. and Aleman, C. *Eur. Polym. J.* **2008**, *44*, 1323–1330.
14. Aradilla, D., Estrany, F., Armelin, E. and Alemán, C. *Thin Solid Films* **2010**, *517*, 4203–4210.
15. Aradilla, D., Pérez-Madrigal, M. M., Estrany, F., Azambuja, D., Iribarren, J. I. and Alemán, C. *Org. Electron.* **2013**, *14*, 1483–1495.

16. Oliver, R., Munoz, A., Ocampo, C., Aleman, C. and Estrany, F. *Chem. Phys.* **2006**, *328*, 299–306.
17. Li, D. Q., Zhu, D. H., Zhou, W. Q., Ma, X. M., Zhou, Q. J., Ye, G. and Xu, J. K. *Int. J. Electrochem. Sci.* **2017**, *12*, 2741–2753.
18. Ma, X. M., Zhu, D. H., Mo, D. Z., Hou, J., Xu, J. K. and Zhou, W. Q. *Int. J. Electrochem. Sci*. **2015**, *10*, 7941–7954.
19. Hu, L., Sun, K., Wang, M., Chen, W., Yang, B., Fu, J., Xiong, Z., Li, X., Tang, X., Zang, Z., Zhang, S., Zhang, S., Sun, L. and Li, M. *ACS Appl. Mater. Interfaces* **2017**, *9*, 43902–43909.
20. Ponder Jr., J. F., Östherholm, A. M. and Reynolds, J. R. *Chem. Mater.* **2017**, *29*, 4385–4392.
21. Jurin, F. E., Buron, C. C., Martin, N., Monney, S. and Filiâtre, C. *Thin Solid Films* **2018**, *664*, 33–40.
22. Kadem, B., Cranton, W., Hassan, A. *Org. Electron.* **2015**, *24*, 73–79.
23. Jurin, F. E., Buron, C. C., Martin, N. and Filiâtre, C. *J. Colloid Interface Sci*. **2014**, *431*, 64–70.
24. Aradilla, D., Estrany, F. and Alemán, C. *J. Phys. Chem. C.* **2011**, *115*, 8430–8438.
25. Banafsheh, B. and Ivey, D. G. *Electrochim. Acta* **2010**, *55*, 4014–4024.
26. Chen, L., Yuan, C., Gao, B., Chen, S. and Zhang, X. *J. Solid State Electrochem.* **2009**, *13*, 1925–1933.
27. Murugan, A. V., Viswanath, A. K., Gopinath, C. S. and Vijayamohanan, K. *J. Appl. Phys.* **2006**, *100*, 074319-6.
28. Fusalba, F., Ho, H. A., Breau, L. and Belanger, D. *Chem. Mater.* **2000**, *12*, 2581–2589.

29. Peng, C., Snook, G. A., Fray, D. J., Shaffer, M. P. and Chen, G. Z. *Chem. Commun.* **2006**, *44*, 4629–4631.

30. Peng, C., Jin, J. and Chen, G. Z. *Electrochim. Acta* **2007**, *53*, 525–537.

31. Fabregat, G., Ballano, G.; Casanovas, J., Laurent, A. D., Armelin, E., del Valle, L. J., Cativiela, C., Jacquemin, D. and Alemán, C. *RSC Adv.* **2013**, *3*, 21069–21083.

32. Fabregat, G., Ballano, G., Armelin, E., del Valle, L. J., Cativiela, C. and Alemán, C. *Polym. Chem.* **2013**, *4*, 1412–1424.

33. Aradilla, D., Estrany, F., Oliver, R. and Alemán, C. *Eur. Polym. J.* **2010**, *46*, 2222–2228.

34. Alemán, C., Casanovas, J., Torras, J., Bertran, O., Armelin, E., Oliver, R. and Estrany, F. *Polymer* **2008**, *49*, 1066–1075.

Table 1. Voltammetric charge and specific capacitance after two consecutive oxidation-reduction cycles (Q_{2nd} and SC_{2nd}, respectively), specific capacitance after fifty redox cycles (SC_{50th}) and percentage difference between SC_{50th} and SC_{2nd} (ΔSC) for the 2- and 4-layered electrodes studied in this work.

2- / 4-layered electrodes	Q_{2nd} **(C)**	SC_{2nd} **(F/g)**	SC_{50th} **(F/g)**	ΔSC **(%)**
PEDOT/PEDOT	0.1636	74	32	-57%
PEDOT/NaCl/PEDOT	0.1724	78	52	-33%
PEDOT/p/PEDOT	0.1951	88	64	-27%
PNMPy/PNMPy	0.1325	85	27	-68%
PNMPy/NaCl/PNMPy	0.2019	129	98	-23%
PNMPy/p/PNMPy	0.0677	43	22	-49%
PEDOT/COP/COP/PEDOT	0.1325	38	28	-26%
PEDOT/COP/NaCl/COP/PEDOT	0.2081	60	43	-28%
PEDOT/COP/p/COP/PEDOT	0.1518	47	39	-17%

CAPTIONS TO FIGURES

Figure 1. Experimental procedure used to prepare (a) PEDOT/NaCl and PEDOT/p single-layered films; (b) PEDOT/NaCl/PEDOT and PEDOT/p/PEDOT 2-layered films; and (c) PEDOT/COP/NaCl/COP/PEDOT and PEDOT/COP/p/COP/PEDOT 4-layered films.

Figure 2. Low (left) and high (right) magnification SEM micrographs of (a) PEDOT, (b) PEDOT/NaCl and (c) PEDOT/p single-layered films.

Figure 3. 3D topographic (left) and 2D height (right) AFM images of (a) PEDOT (20×20 μm^2) and (b) PEDOT/NaCl (13.7×12 μm^2). Cross-sectional profiles were recorded at the indicated positions.

Figure 4. Low (left) and high (right) magnification SEM micrographs of (a) PNMPy, (b) PNMPy/NaCl and (c) PNMPy/p single-layered films.

Figure 5. 3D topographic (left) and 2D phase (right) AFM images of (a) PNMPy, (b) PNMPy/NaCl and (c) PNMPy/p single-layered films. Images are 20×20 μm^2 in all cases.

Figure 6. Low (left) and high (right) magnification SEM micrographs of (a) COP, (b) COP/NaCl and (c) COP/p single-layered films.

Figure 7. 3D topographic (left) and 2D phase (right) AFM images of (a) COP, (b) COP/NaCl and (c) COP/p single-layered films. Images are 25×25 μm^2 in all cases.

Figure 8. (a) FTIR and (b) UV-vis spectra of PEDOT/PEDOT, PEDOT/NaCl/PEDOT and PEDOT/p/PEDOT

Figure 9. First control voltammogram (solid lines) and voltammogram after 50 consecutive oxidation and reduction cycles (dashed lines) of: (a) PEDOT/PEDOT, PEDOT/NaCl/PEDOT and PEDOT/p/PEDOT; and (b) PNMPy/PNMPy, PNMPy/NaCl/PNMPy and PNMPy/p/PNMPy. Voltammograms were recorded in

acetonitrile with 0.1 M $LiClO_4$ at 50 mV/s and at room temperature. Initial and final potentials: -0.50 V. Reversal potential: 1.60 V.

Figure 10. First control voltammogram (solid lines) and voltammogram after 50 consecutive oxidation and reduction cycles (dashed lines) of PEDOT/COP/COP/PEDOT, PEDOTCOP//NaCl/COP/PEDOT and PEDOT/COP//p/COP/PEDOT. Voltammograms were recorded in acetonitrile with 0.1 M $LiClO_4$ at 50 mV/s and at room temperature. Initial and final potentials: -0.50 V. Reversal potential: 1.60 V.

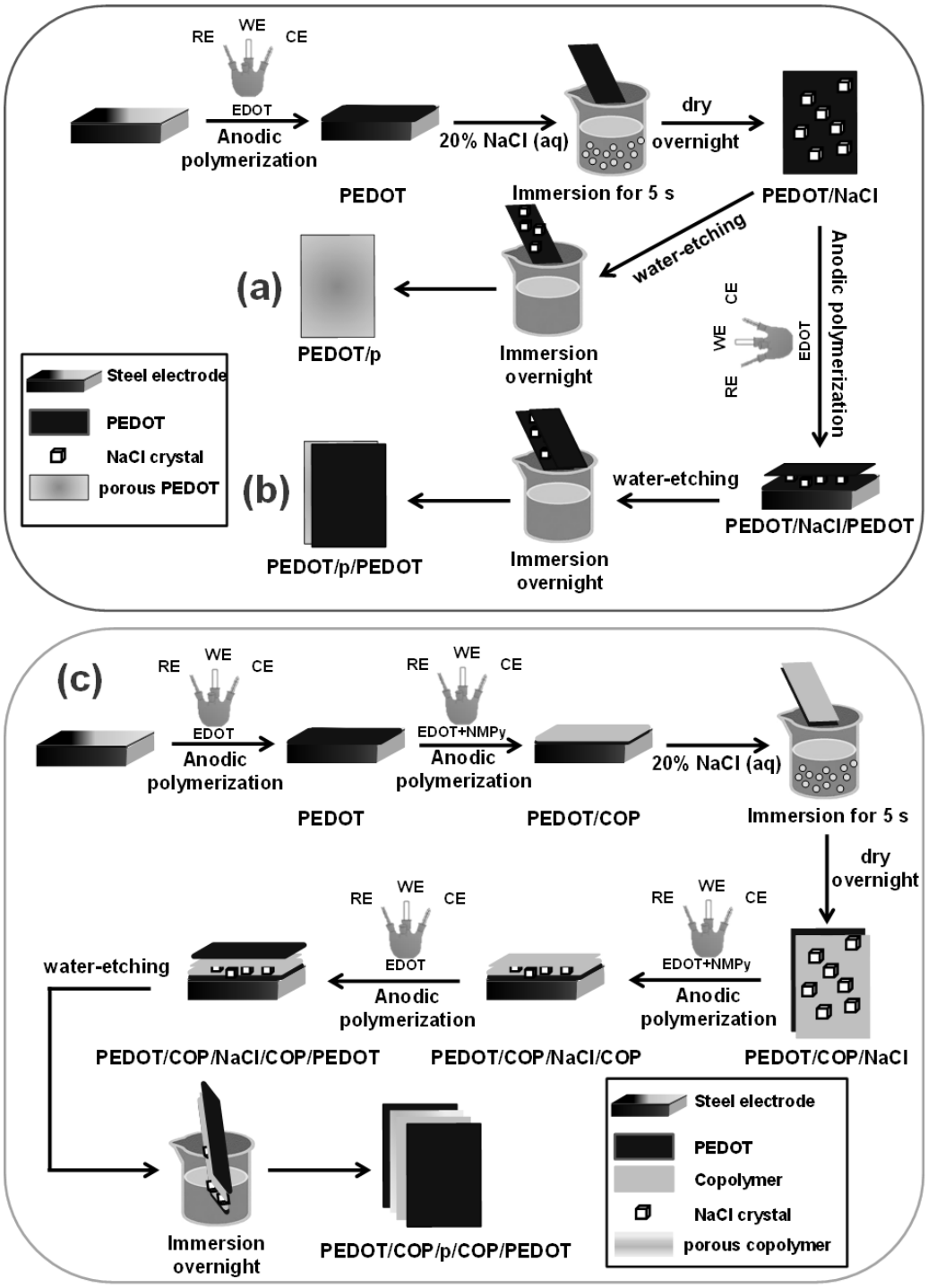
RE
WE
CE
EDOT
Anodic polymerization
PEDOT
20% NaCl (aq)
Immersion for 5 s
dry overnight
PEDOT/NaCl
water-etching
Anodic polymerization
(a)
PEDOT/p
Immersion overnight
Steel electrode
PEDOT
NaCl crystal
porous PEDOT
(b)
PEDOT/p/PEDOT
water-etching
PEDOT/NaCl/PEDOT
(c)
EDOT+NMPy
PEDOT/COP
PEDOT/COP/NaCl
PEDOT/COP/NaCl/COP
PEDOT/COP/NaCl/COP/PEDOT
Copolymer
porous copolymer
PEDOT/COP/p/COP/PEDOT

Figure 1

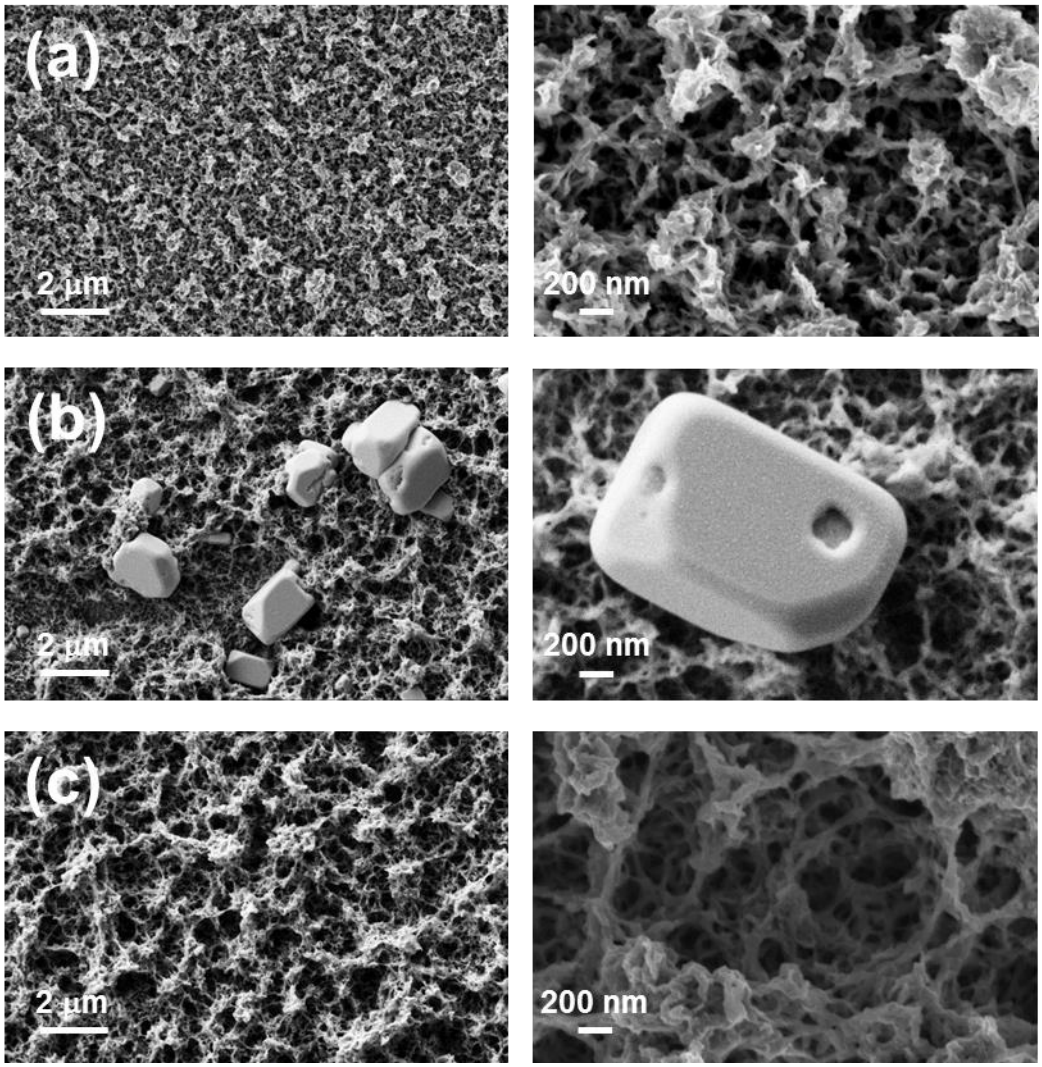

Figure 2

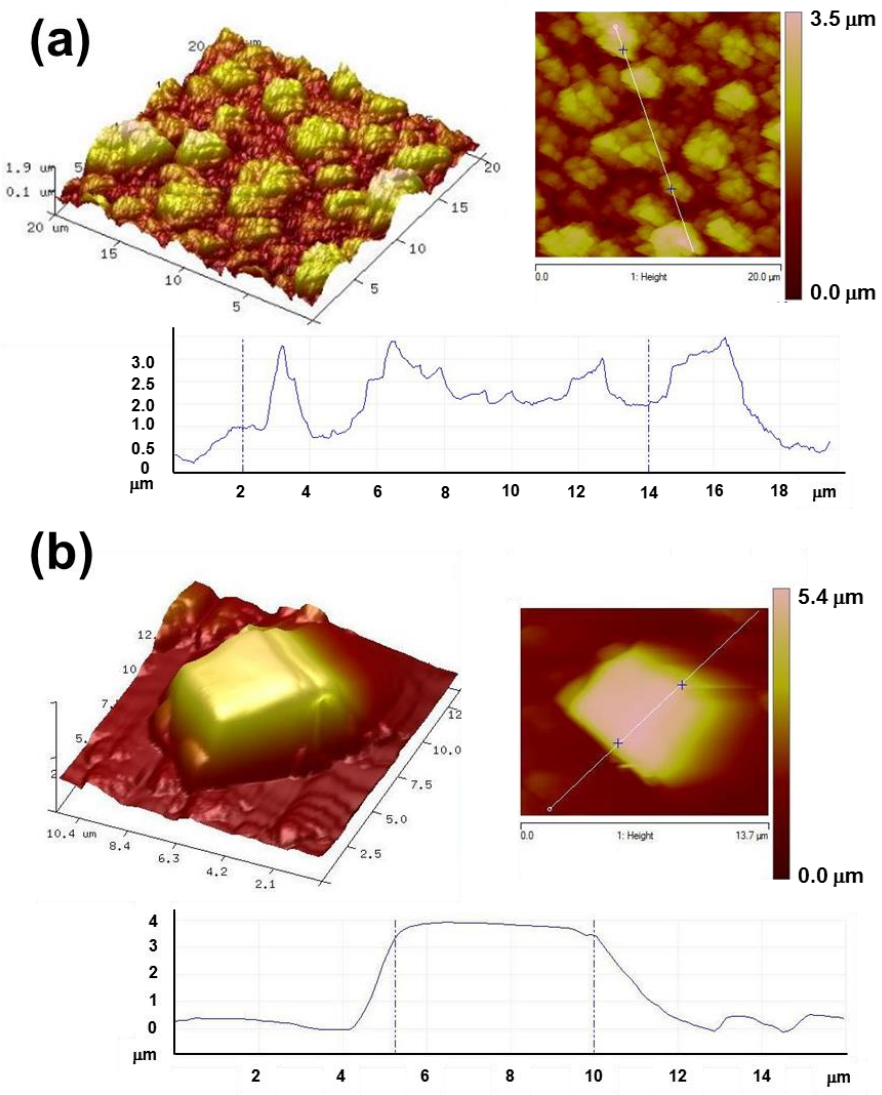
(a)
3.5 µm
0.0 µm
1: Height
3.0
2.5
2.0
1.0
0.5
0
µm
2
4
6
8
10
12
14
16
18
µm
(b)
5.4 µm
0.0 µm
1: Height
4
3
2
1
0
µm
2
4
6
8
10
12
14
µm

Figure 3

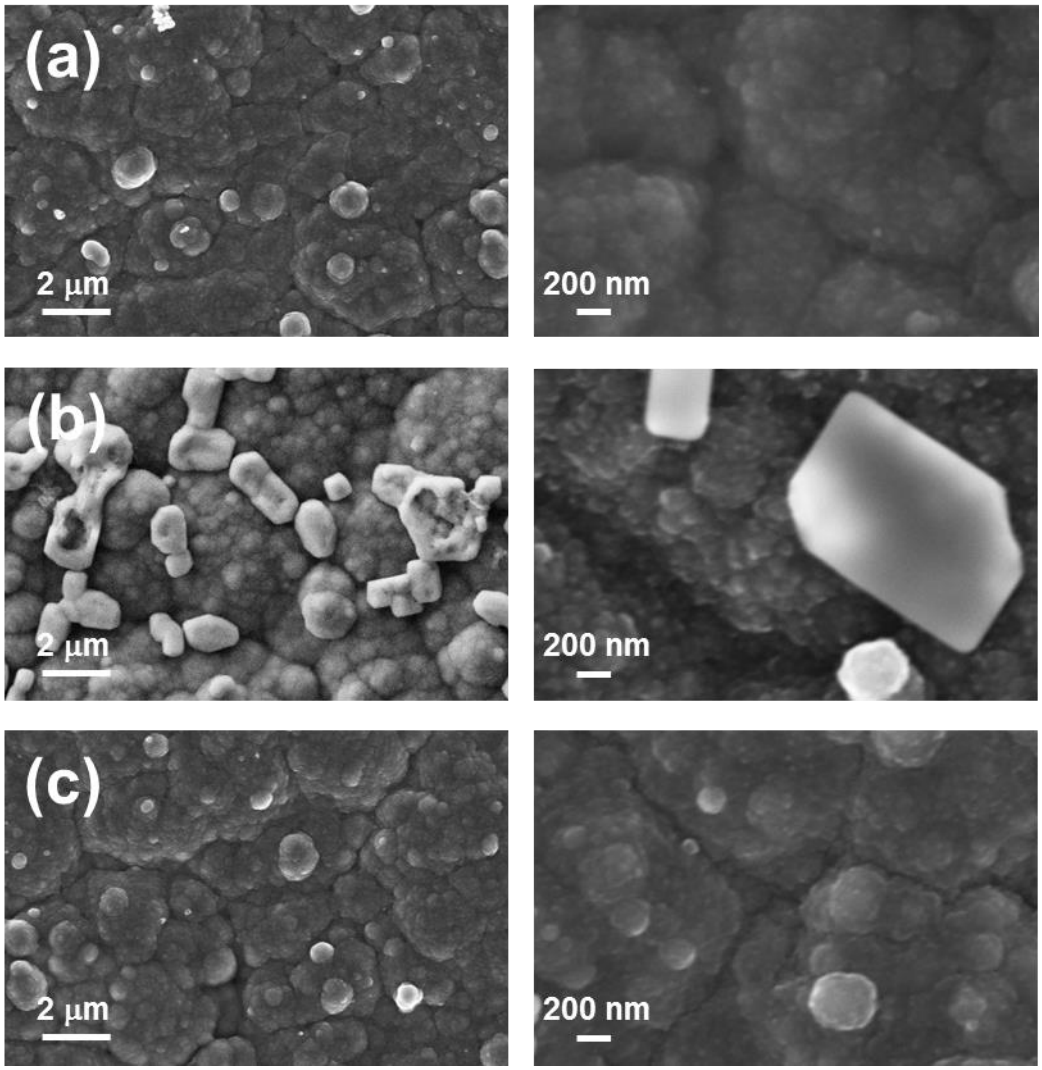

Figure 4

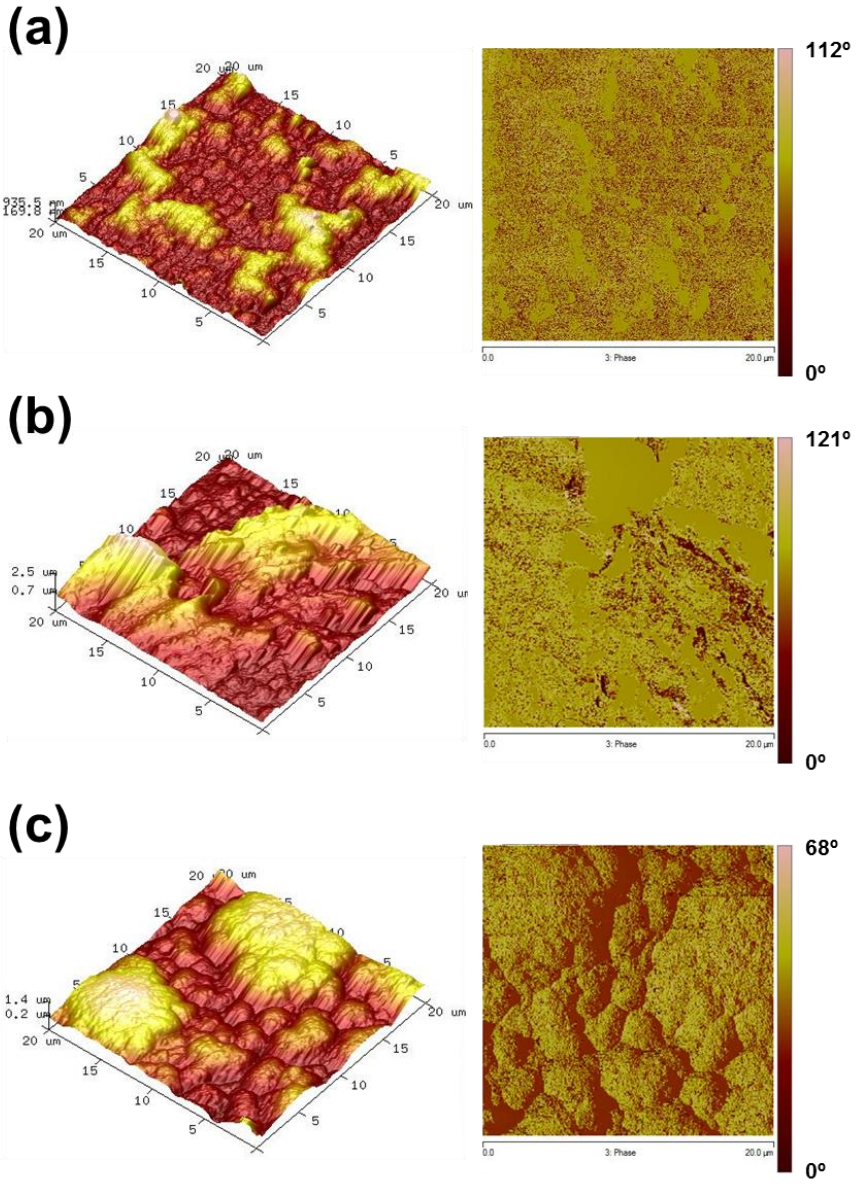

Figure 5

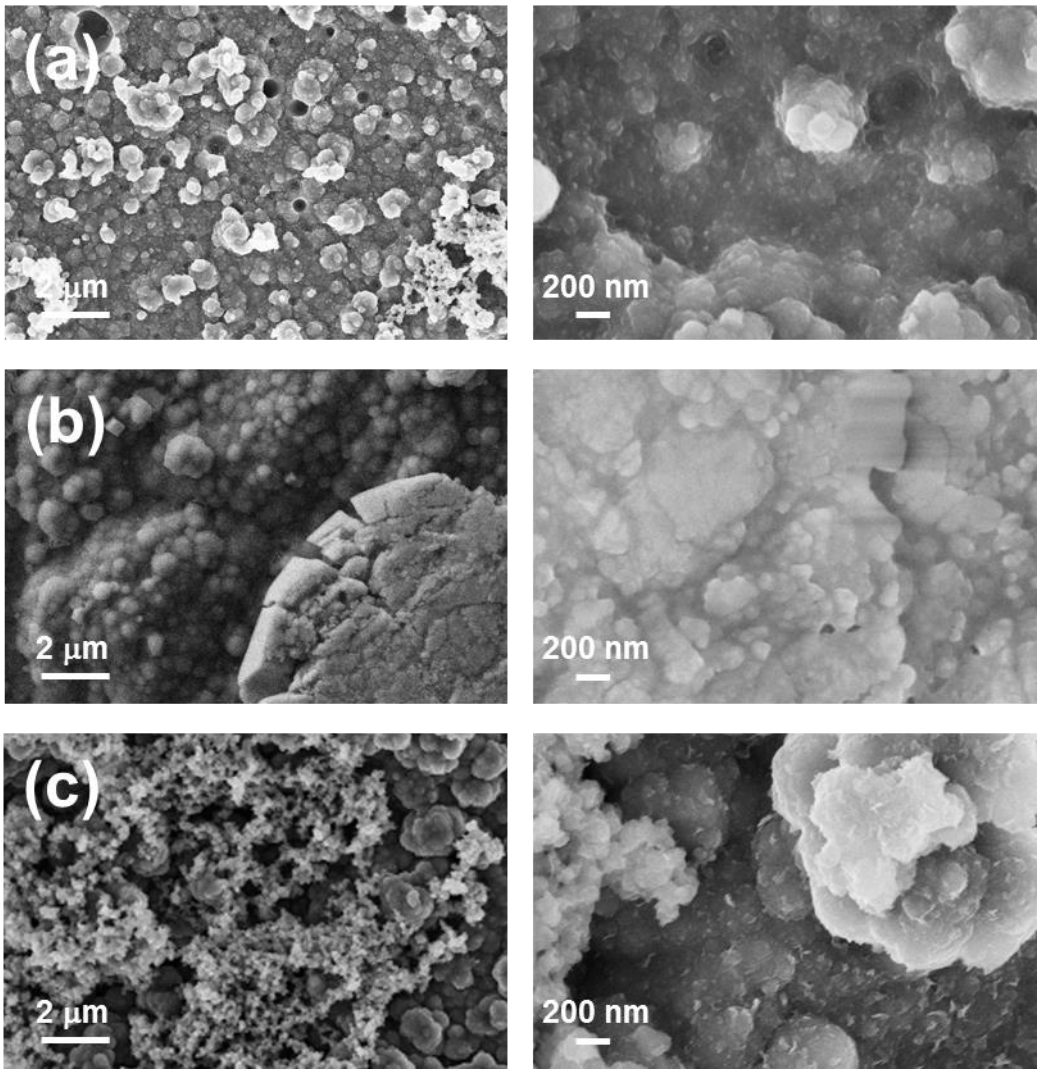

Figure 6

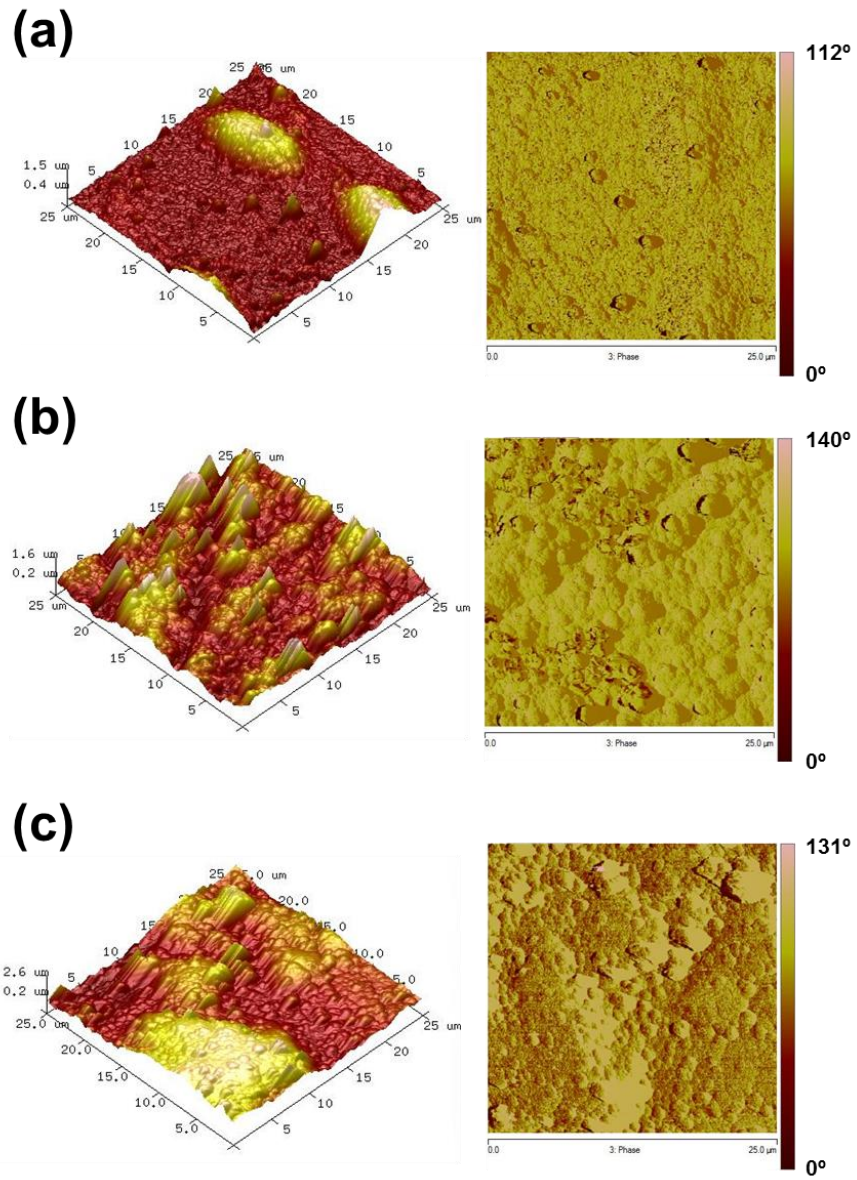
(a)
1.5 um
0.4 um
25 um
112°
0°
(b)
1.6 um
0.2 um
25 um
140°
0°
(c)
2.6 um
0.2 um
25.0 um
131°
0°

Figure 7

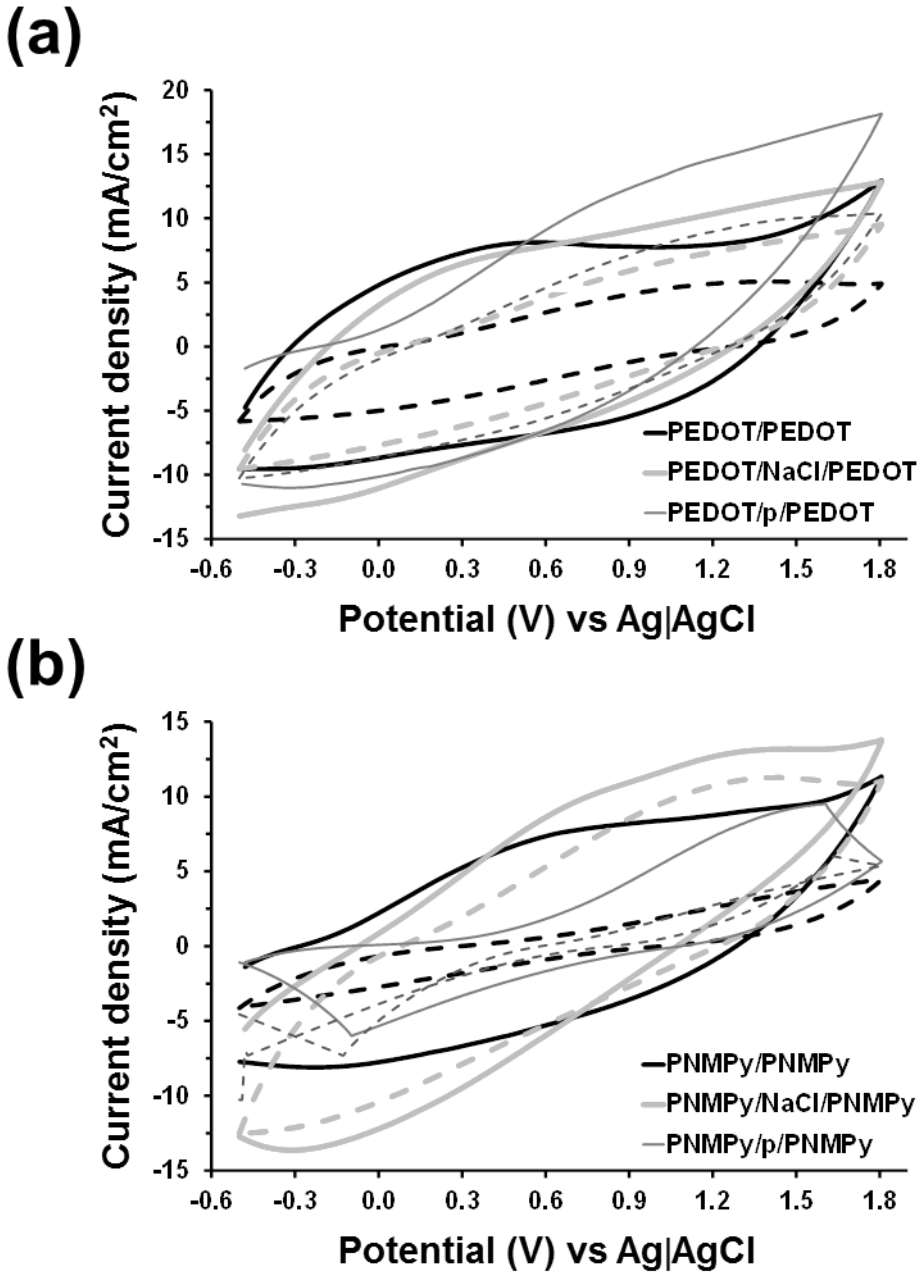
(a)
Current density (mA/cm²)
20
15
10
5
0
-5
-10
-15
-0.6
-0.3
0.0
0.3
0.6
0.9
1.2
1.5
1.8
Potential (V) vs Ag|AgCl
PEDOT/PEDOT
PEDOT/NaCl/PEDOT
PEDOT/p/PEDOT
(b)
Current density (mA/cm²)
15
10
5
0
-5
-10
-15
-0.6
-0.3
0.0
0.3
0.6
0.9
1.2
1.5
1.8
Potential (V) vs Ag|AgCl
PNMPy/PNMPy
PNMPy/NaCl/PNMPy
PNMPy/p/PNMPy

Figure 8

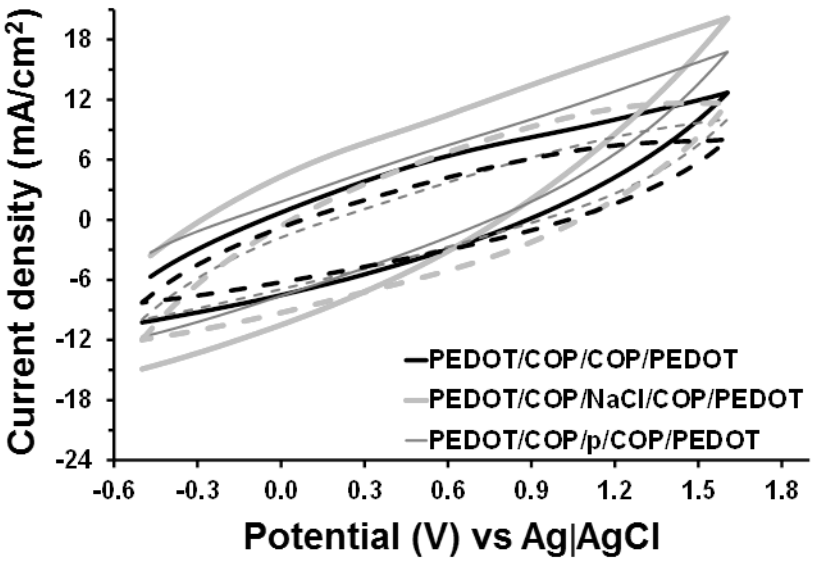
Current density (mA/cm²)
18
12
6
0
-6
-12
-18
-24
-0.6
-0.3
0.0
0.3
0.6
0.9
1.2
1.5
1.8
Potential (V) vs Ag|AgCl
PEDOT/COP/COP/PEDOT
PEDOT/COP/NaCl/COP/PEDOT
PEDOT/COP/p/COP/PEDOT

Figure 9

GRAPHICAL ABSTRACT